OPEN

Microsystems & Nanoengineering (2015) 1, 15010; doi:10.1038/micronano.2015.10

www.nature.com/micronano

ARTICLE

Extracellular matrix-based intracortical microelectrodes: Toward a microfabricated neural interface based on natural materials

Wen Shen[1,4], Lohitash Karumbaiah[2], Xi Liu[3], Tarun Saxena[2], Shuodan Chen[1], Radhika Patkar[2], Ravi V. Bellamkonda[2] and Mark G. Allen[1,4]

Extracellular matrix (ECM)-based implantable neural electrodes (NEs) were achieved using a microfabrication strategy on natural-substrate-based organic materials. The ECM-based design minimized the introduction of non-natural products into the brain. Further, it rendered the implants sufficiently rigid for penetration into the target brain region and allowed them subsequently to soften to match the elastic modulus of brain tissue upon exposure to physiological conditions, thereby reducing inflammatory strain fields in the tissue. Preliminary studies suggested that ECM-NEs produce a reduced inflammatory response compared with inorganic rigid and flexible approaches. *In vivo* intracortical recordings from the rat motor cortex illustrate one mode of use for these ECM-NEs.

Keywords: bio-MEMS; electrophysiology; extracellular matrix; finite element analysis; immunohistology; intracortical neural microelectrodes; stress; tissue-compliant electrodes

Microsystems & Nanoengineering (2015) **1,** 15010; doi:10.1038/micronano.2015.10; Published online: 29 June 2015

INTRODUCTION

Implantable neural prosthetic devices (NPDs) allow direct interfacing with local neuronal populations and form key components of brain–computer interfaces (BCIs)[1]. Current state-of-the-art NPDs in use, particularly in clinical settings, are typically made of silicon or noble metals[2,3]. They have led to many significant advances such as neural recordings, deep brain stimulation, and brain-controlled prosthetic devices[4–7]. However, these silicon- and metal-based devices are unable to sustain communication with neurons over long periods of time.

One of the primary challenges that impedes the sustained functionality of these NPDs is the mechanical mismatch between the soft neural tissue and the rigid NPDs, which results in large strains and causes local inflammation at the NPD–tissue interfaces. To address this limitation, NPDs made from materials with lower Young's moduli have been employed (e.g., flexible polyimide or parylene materials)[8,9]. However, the Young's moduli, E, of these materials (i.e., $E_{\text{polyimide}} \approx 2.5$ GPa[10], $E_{\text{ParyleneC}} \approx 2.8$ GPa[11]) are still six orders of magnitude higher than that of brain tissue ($E_{\text{brain}} \approx 5.51$ kPa[12]). Given certain device dimensions, a further reduction in the mechanical modulus of the materials comprising the device is expected to provide a more tissue–complaint interface, thereby lowering the strains induced on the tissue. Kipke *et al.* showed that a hypothetical 'soft' neural prosthetic electrode with an E of 6 MPa would reduce the strain induced at the tissue–device interface by up to two orders of magnitude compared with silicon-based electrodes[12]. Capadona *et al.* showed that electrodes formed from a PVA-coated tunable cellulose nanocrystal (tCNC) nanocomposite that demonstrated an E of 12 MPa in its "soft" (hydrated) state resulted in a 30%–50% reduction in interfacial micromotion-induced stress compared with bare silicon-based electrodes[13].

Soft/flexible NPDs face a materials challenge because they must also be sufficiently stiff to penetrate and reach the desired position within the neural tissue while minimizing stress and damage. Integrating stiff insertion devices with the NPDs could facilitate the delivery of flexible NPDs into the brain tissue[9,14] but may inadvertently damage the brain tissue during insertion and retraction. Incorporating ultrasonic vibration or utilizing ultra-high speeds during insertion showed initial success with silicone-based and polyimide-based flexible devices[15,16]. However, it still remains a challenge to implant ultra-soft devices with a Young's modulus similar to that of brain tissue. To address this challenge, it is possible to utilize materials that are relatively stiff in an unhydrated state, but which achieve substantial compliance upon hydration. For example, Weder *et al.* demonstrated that compliant implantable neural electrodes (NEs) based on PVA-coated tCNC nanocomposite materials reduced acute and chronic neuro-inflammatory responses in comparison with stiff Si-based NEs[17–19]. These PVAc-tCNC electrodes are initially rigid in their dry state to accommodate implantation but become compliant in their "soft" (hydrated) state after implantation[18].

Another major challenge is biocompatibility at the NPD–tissue interface. NPDs are typically composed of materials foreign to their implanted environment, resulting in a sustained glial response that eventually leads to neurodegeneration and decreases the fidelity of the recorded neural signals[20–22]. In assessing biocompatibility, it is constructive to consider the extracellular matrix (ECM) environment of neuronal cells, as the ECM comprises a notable portion of the central nervous system (CNS) and supports critical functions in normal physiology. The

[1]Institute for Electronics and Nanotechnology, Georgia Institute of Technology, Atlanta, GA 30332, USA; [2]Wallace H Coulter Department of Biomedical Engineering, Georgia Institute of Technology & Emory School of Medicine, Atlanta, GA 30332, USA; [3]George W. Woodruff School of Mechanical Engineering, Georgia Institute of Technology, Atlanta, GA 30332, USA and [4]Krishna P. Singh Center for Nanotechnology, University of Pennsylvania, Philadelphia, PA 19104, USA
Correspondence: Professor Mark G. Allen (mallen@seas.upenn.edu)
Received: 31 January 2015; revised: 10 May 2015; accepted: 15 May 2015

ECM of brain tissue mainly comprises laminin, fibronectin, and collagen; these proteins form the interstitial matrix and the basement membrane[23]. It has been found that ECM materials, when acting as coatings and scaffolds, can enhance neural interfacing by forming a naturally biocompatible substrate for promoting neural regeneration, growth, and function[24–27]. Furthermore, these molecules can modulate the immune response and reduce inflammation and glial scar formation[23,25,28]. Moreover, studies have shown that ECM materials support neural cell viability, proliferation and regeneration[29–31].

Incorporation of ECM materials into neural electrodes is therefore expected to provide natural biochemical cues to direct neural growth and function and potentially minimize the inflammatory responses and biocompatibility concerns associated with NPDs. Biomolecule-based coatings[32,33] including ECM molecules and anti-inflammatory drugs[34] have been implemented on NPD surfaces and showed initial improvement in promoting neural cell growth and preventing glial scar formation at the tissue–device interfaces, ultimately enhancing neuronal attachment and promoting good initial recordings *in vivo*. However, these results were unsustainable at longer time scales and, thus, could not support chronic neural interfacing[35,36].

The mechanical compatibility and biocompatibility of ECM-based materials suggest that a fruitful direction for further enhancing the compatibility of NPDs with neural tissue might be to fabricate almost the entire NPD from ECM material, rather than using ECM just as a coating. Such an approach will require the development of new fabrication technologies to realize electrically functionalized constructs made primarily from protein.

Microfabrication of ECM proteins to form micro-sized NPDs is a technology challenge because these materials are sensitive to the harsh solvents and high temperatures of conventional microfabrication processes. While previous studies have successfully prepared 3D scaffolds based on *in situ* collagen assembly[37–39] and bulk collagen gel[40], the development of microfabrication processes for preparing electrically functional ECM-based NPDs is still required. In this study, we aim to demonstrate the fundamental possibility of constructing implantable NPDs primarily from ECM proteins. Such NPDs would feature both materials compatibility and mechanical compliance with neural tissue while introducing a minimum volume of foreign material into the neural tissue. Further, unlike coating-based approaches, ECM electrodes contain a relatively large amount of natural material, which may support the device–neural interface over longer time periods.

Using ECM-compatible microfabrication techniques, we have addressed the fabrication challenges to create electrically functional ECM-based NPDs. The fabrication process is compatible with various protein hydrogels and supports the integration of biological materials in microelectronic devices. As a case study, we present the fabrication of collagen- and Matrigel-based intracortical NEs. Collagen is an ECM protein that is critical in the formation of connective structures in tendons, organs, and basement membranes and features long fibrils and 3D structures with high tensile strengths. In this study, collagen is used as a biocompatible substrate because its higher mechanical strength can support initial insertion while softening after implantation. Matrigel, a gelatinous ECM protein mixture resembling the complex extracellular neuronal environment, is used to provide a more neuronal-compatible substrate. Successful implantation and tissue-compliance were demonstrated by insertion force-displacement measurements and a finite element model analysis, respectively; the functionality of the implants was verified by electrophysiological recordings of neural activity from the rat motor cortex region upon whisker stimulation; and their neural tissue compatibility was demonstrated by immunohistological studies.

MATERIALS AND METHODS

Materials

The collagen films that are ultimately used as substrates for further processing were prepared prior to their fabrication and integration with the NE electronics. The process began with Type I bovine collagen in a 3 mg mL^{-1} solution (Advanced BioMatrix, Carlsbad, CA, USA). The collagen was gently mixed with 10X phosphate-buffered saline (PBS) and 0.1 M NaOH at a ratio of 13:2:1 by volume until small fragments of collagen started to form. The mixed collagen solution was then cast into an acrylic mold, followed by polymerization at 37 °C and 96% humidity for four days, yielding uniform collagen gels (thickness of 40 mm). These collagen gels were then dried on glass slides in air at 37 °C for 24 h followed by multiple rinses with DI water and air drying, forming dried collagen films (thickness of 40 μm). The collagen films were subsequently removed from the acrylic mold and glass slides for subsequent use as substrates. The entire process was carried out under sterile conditions. Basement Membrane Matrix Matrigel (BD Bioscience, Frankline Lakes, NJ, USA) was diluted with PBS solution to a concentration of 2 mg mL^{-1} and was used for subsequent fabrication of ECM-NEs.

Parylene/conductor film fabrication

Patterned conductors comprised metal electrodes encapsulated by an ultrathin parylene film that was used as a small internal "core" within the ECM-NEs. The parylene/conductor cores were prepared on silicon substrates using standard batch microfabrication procedures: a 3-μm-thick Parylene C (poly-monochloro-para-xylylene) (Specialty Coating Systems, Indianapolis, IN, USA) film was deposited on a silicon carrier wafer by chemical vapor deposition (SCS Labcoater, Special Coating Systems, Inc., Indianapolis, IN, USA) (Figure 1a). Au (400 nm) was then deposited using electron beam evaporation and patterned by lift-off, yielding interconnecting lines and pads (Figure 1b). Another thin layer of Parylene C (3 μm) was deposited and then patterned by reactive ion etching, leaving only the pads at the ends of the lines exposed (Figure 1c).

Electrodeposition of nanoporous Pt

Because electrical connections to these NEs are required for functionality, the fabrication proceeded by first electrically connecting the parylene/conductor core structures fabricated as described above to nano-strip neural connectors (Omnetics Connector Corporation, Minneapolis, MN, USA). To increase the effective area and in turn lower the electrochemical impedance of the recording sites, nanoporous Pt black was deposited on the sites (Figure 1d and Supplementary Figure S1): 20 mL electrolyte containing 1% chloroplatinic acid, 0.005% lead acetate, and 0.01 M HCl mixed in DI water was used for electroplating of the nanoporous Pt. The parylene/conductor core was pre-treated in an oxygen plasma using reactive ion etching for 1 min and then immersed in the electrolyte with a Pt anode. A pulsed current of −45 μA was first applied for 80 ms and then reduced to zero for 80 ms; this current cycle was repeated 300 times.

Microfabrication of the ECM-NE devices

To fabricate parylene/conductor cores that are embedded within the ECM yet allow the electrode surfaces to be exposed, a magnetically assisted micropatterning technique was utilized. A polydimethylsiloxane (PDMS) substrate was prepared with two features: a recess for the Omnetics connector, and a micromagnet embedded in the volume of the PDMS underlying the area into which the electrode region would subsequently extend. A collagen film was placed on the PDMS substrate over the latter region. The Pt-coated parylene cores were sterilized and individually transferred onto the collagen film in an aligned fashion. A steel

 doi:10.1038/micronano.2015.10

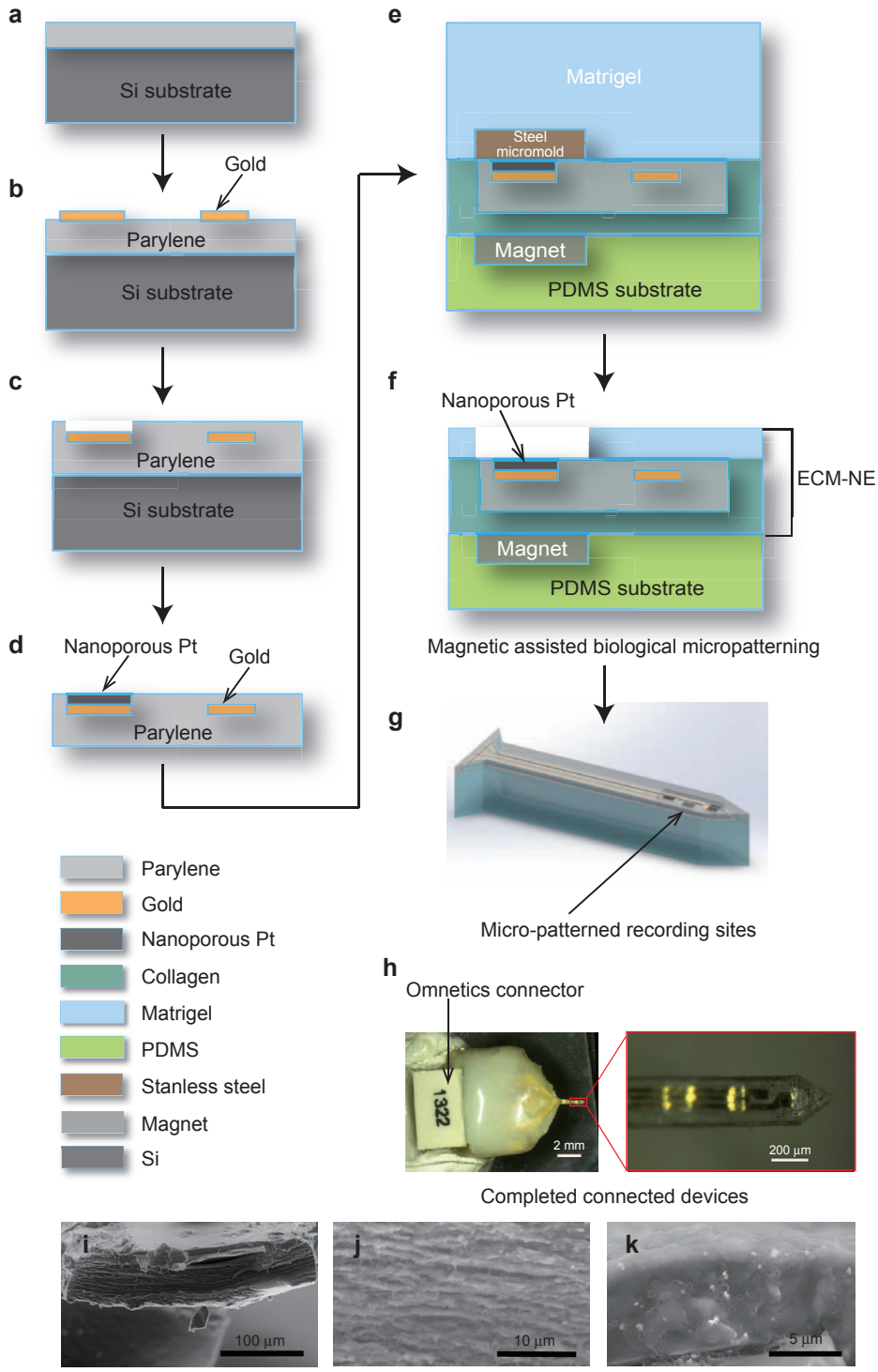

Figure 1 Steps for fabricating ECM-based intracortical neural microelectrodes. (**a**)–(**c**) Steps for fabricating the ultra-thin parylene/conductor core; (**d**) electrochemical deposition of nanoporous Pt on the recording sites; (**e**)–(**f**) magnetic-assisted micropatterning of the top Matrigel layer; (**g**) illustration of the ECM-NEs after laser ablation. (**h**) A representative ECM-NE device and an enlarged view of the electrode tip. (**i**)–(**k**) SEM images of the cross-sectional areas of ECM-NEs: (**i**) the full device; (**j**) collagen; and (**k**) Matrigel.

mask was placed on top of the recording site and held in place by the PDMS-embedded magnet (Figure 1e). Matrigel (2 mg mL^{-1}, 4 ℃) was then brought to room temperature and cast onto the electrode on the PDMS mold. The Matrigel formed a gel within a few minutes of being heated to room temperature. After the gel formed, the steel masks were removed using a magnetized needle tip, exposing the recording sites (Figure 1f). As the remaining Matrigel dried, it adhered to the underlying collagen substrate to form an integrated structure with a total thickness of 50 μm. The Matrigel/collagen composite was then transferred to a

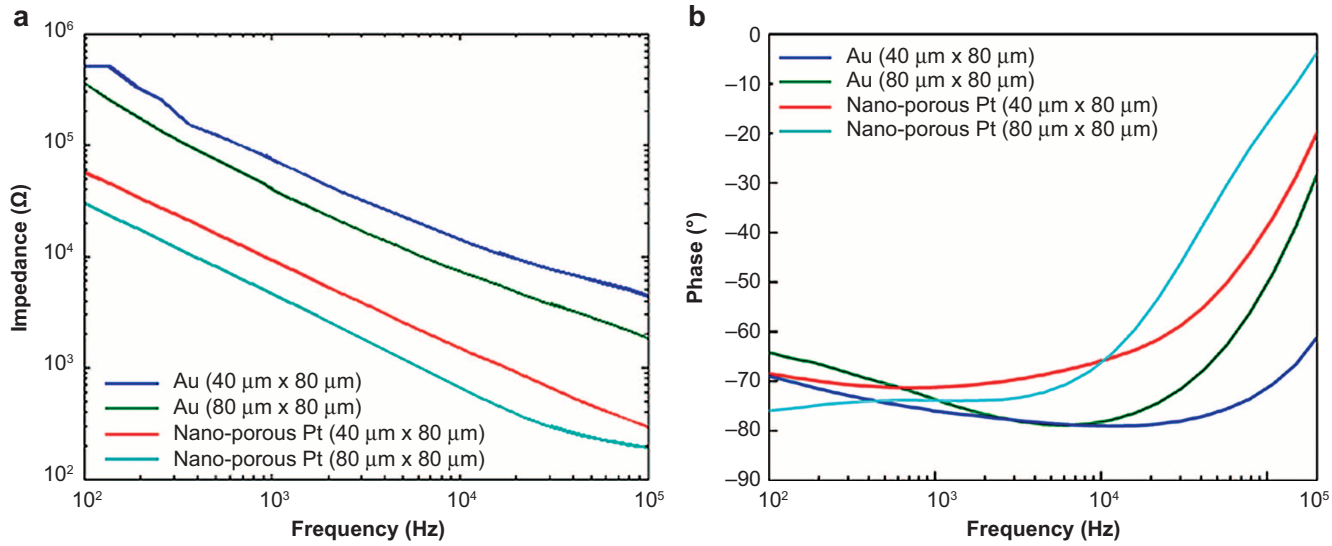

Figure 2 Electrochemical impedance spectroscopy (EIS) of the ECM-NEs: (**a**) magnitudes; (**b**) phase angles.

glass substrate and processing was completed by ablation of the electrode shank dimensions using a UV excimer laser. The reason for the replacement of the PDMS substrate with a glass substrate is to avoid any redeposition of PDMS debris from the laser ablation. These ECM-NEs consist of a single shank, 2 mm in length and 310 μm in width, each bearing a three-electrode configuration. Two electrodes have recording site dimensions of 40 × 80 μm each, and one electrode has a recording site dimension of 80 × 80 μm. All the recording sites were included within a 450 μm region, corresponding to the span of the Layer IV region of the rat barrel cortex. Similar ECM-NEs used for tissue compatibility studies were fabricated with the same dimensions but were not connected to connectors and were not deposited with nanoporous Pt at the recording sites, nor did they contain micropatterned Matrigel.

Electrochemical impedance spectroscopy (EIS)

EIS measurements were made using a lock-in amplifier with custom MATLAB software. To obtain *in vitro* EIS measurements, each electrode was submerged in a 1X PBS solution with a stainless steel wire serving as the counter electrode. Impedance measurements were taken between 100 Hz and 100 kHz at 10 mV.

Nanoindentation

Nanoindentations were conducted using a Hysitron TriboIndenter (Hysitron, Inc., Eden Prairie, MN, USA) equipped with a fluid cell probe. Five to ten indentations, each at least 5 mm apart, were taken on each collagen film sample. A 1500 μN load was applied with both loading and unloading rates of 150 μN s^{-1} for measuring the dry collagen films. For the wet collagen film measurements, each collagen film was immersed in DI water at room temperature. After at least 10 min, to allow the collagen films to become fully hydrated, the measurements began by first calibrating for the effect of the interaction of the nanoindenter tip with the liquid, followed by the application of a 20 μN load with both loading and unloading rates of 2.5 μN s^{-1}.

Determination of the buckling force

The critical buckling force (F) of the NEs during the insertion process was calculated from a simple Euler criterion:

$$F = \frac{\pi^2 EI}{(KL)^2} \quad (1)$$

where E is the elastic modulus, I is the area moment of inertia, L is the length of the electrode shank, and K is the column effective length factor. Because for the devices fabricated here the product EI of the collagen dominates (owing to the very small relative thicknesses of the other components, the high-order dependence of the moment of inertia on thickness, and the fact that the collagen is in the unhydrated stiff state during insertion), this simple model provided sufficient design guidance for these devices.

Insertion force measurement

To examine the ability of these NEs to be implanted into brain tissue, we carried out experiments using a 2% SeaPrep agarose gel as a brain tissue substitute. The insertion force was measured using a Bose ElectroForce 3100 test instrument equipped with a 0.5 N load cell. Ten samples were used for the ECM-NEs measurements, and at least four samples were used for the PDMS-NEs and Si-NEs measurements.

Finite element analysis (FEA)

A three-dimensional (3D) model of the NEs–tissue interface was developed in ANSYS ® Ver.15 (ANSYS, Inc., Canonsburg, PA, USA) to quantitatively map the strain field induced by brain micromotion between the brain tissue and various NE devices (ECM-NEs, PDMS-NEs, and Si-NEs) in a post-implantation state. The geometry and dimensions of the composite ECM-NEs are shown in Supplementary Figure S2a, and those for the corresponding stiff-synthetic analog (Si-NEs) and soft-synthetic analog (PDMS-NEs) are shown in Supplementary Figure S2b. The model consists of two parts: the brain tissue and the NE implanted in the brain. The cerebral cortex is approximated as a linear elastic model for simulating the small strains in the brain. The region of interest (ROI) in the brain was chosen to be much larger than the region affected by the strain field induced by the implanted NEs. A full

doi:10.1038/micronano.2015.10

model was simulated to include the effects in all directions, and the geometry of the NEs used in the simulation is provided in Supplementary Figure S3. The initial conditions were defined such that the NE had already been implanted in the brain tissue and the NE shank and brain tissue were in contact with each other. The extremities of the ROI were set to a fixed reference, simulating attachment of the brain tissue to the body, thereby avoiding any large-scale global displacement while allowing local displacement around the implantation site. The displacement magnitudes were chosen by considering the typical displacements associated with rat brain motion during physiological activity relative to an NE fixed at the skull; typical motional displacements were on the order of microns. To simulate different degrees of physical coupling between the implanted NEs, NE-tissue friction coefficients varying from 0 to 1 and a perfect bond condition were used.

Animal experiments

All animal procedures were approved by the Institutional Animal Care and Use Committees (IACUC, USA) at the Georgia Institute of Technology. A total of 32 adult male Sprague-Dawley rats (10–12 weeks old, ~250 gm) were implanted with electrodes and allowed to survive for three days or 16-week post-implantation (16 WPI). Eight animals were used for the electrophysiological recordings; and 24 animals were used for the histological analysis. The surgical and stimulation methods were as previously described[41]. Briefly, for each of these procedures, a single rat was anesthetized using 2% isoflurane and a continuous infusion of isoflurane. Lidocaine was injected subdermally as a local anesthetic. The animal's body temperature was regulated via feedback-controlled heating, and its heart rate and respiration were monitored throughout the procedure. A craniotomy was made ~1.5 mm posterior from the anterior bregma and ~4 mm lateral from the midline, followed by the placement of four bone screws, 2 anterior to the bregma and 2 posterior to the lambda. The dura mater was subsequently removed and the electrode was stereotaxically implanted to a depth of 1200 μm in the rat barrel cortex. The craniotomy was covered with sterile 2% SeaKem agarose (Lonza, Allendale, NJ, USA) and sealed with UV-curing dental cement, which was also used to build the head cap. The hemostats were subsequently removed and the skin flap sutured back. The animal was injected with buprenorphine HCl and allowed to recover before being returned to its cage.

Histology

Three days or 16 weeks after electrode implantation, animals were transcardially perfused with PBS, followed by 4% paraformaldehyde, followed by 30% sucrose in PBS (300 mL each), and brain tissue for immunohistochemical analysis (n = 6/electrode type) was sectioned as described previously[42]. Multiple electrode types were analyzed to compare the ECM-NEs with a synthetic analog (PDMS-NEs). All the images were collected using a Zeiss Axiovert 200 M (Carl Zeiss, Thornwood, NY, USA) fluorescence microscope using equal exposure times for fluorescent markers. The images were normalized by subtracting the intensity of a naïve section stained with the appropriate secondary antibody and imaged at the same exposure time. Each implant footprint was manually defined, and the fluorescence intensity as a function of distance from the implant site was calculated using the MATLAB Image Processing Toolbox (MathWorks, Natick, MA, USA) as previously described[41,42]. The ROI was defined as the region 100 μm away from the perimeter of the implant footprint surface. The integral of the fluorescent intensity, which was defined as the total fluorescent intensity within the ROI, was calculated, and normalized integral fluorescent intensities were obtained for the immunohistochemical assays. The neuron population within the ROI was manually counted, and the number of neurons per ROI area was then calculated.

Data acquisition and processing

All the animal electrophysiological data were acquired using an OmniPlex D neural data acquisition system (Plexon Inc., Dallas, TX, USA). The ECM-NEs were connected through an interface board to the Plexon system. The signals were sampled at 40 kHz sampling rate per channel. The high-pass filter was set at 300 Hz, and the low-pass filter was set at 8 kHz. Before each recording, the system was tested for artifacts caused by the fluctuation of air caused by finger movements close to the animal. Animal whisker stimulation was conducted non-continuously using a non-conductive wooden stick. The neural recordings were analyzed offline using Offline Sorter (OFS) (Plexon Inc.) using a standard E-M t-distribution clustering algorithm. The signal-to-noise ratio (SNR) was calculated as the square of the peak-to-peak amplitude of the mean waveform of the cluster divided by three times the standard deviation, and the cut-off SNR was set to 1.25.

RESULTS

Electrochemical impedance spectroscopy (EIS)

The EIS spectrum over the frequency range from 100 Hz to 100 kHz is shown in Figure 2. At low frequencies, the impedance and phase are dominated by double layer characteristics and show a more capacitive response. As expected, NEs with larger recording site sizes show lower impedances, and the nanoporous Pt-coated NEs further lower the impedance to ~10 kΩ for the NEs with 40 × 80 μm^2 recording sites and to ~5 kΩ for the NEs with 40 × 80 μm^2 recording sites at 1 kHz, which is a physiologically relevant neuron spiking frequency. The EIS measurements verified that the dehydration and rehydration of the ECM-NEs did not affect the impedance of the electrodes (results not shown).

Insertion

Although hydrated ECM materials are soft and have a E close to that of brain tissue, the dehydrated (dry) collagen film shows a significantly increased E of ~ 3.4 ± 0.28 GPa (Figure 3a) owing to tighter molecular packing of the collagen microfibrils[43]. This high E allows the ECM-NEs to have a high resistance to buckling in the axial direction normal to the brain surface, increasing the ease of implantation[44]. The critical buckling force of the dehydrated ECM-NEs is 2.87 × 10^{-2} N, comparable to that of commercial Si-based devices (Michigan M50, NeuroNexus Technologies, Inc., Ann Arbor, MI, USA) (5.42 × 10^{-2} N), and three orders of magnitude higher than that of flexible PDMS-based NEs with the same dimensions (1.69 × 10^{-5} N). The insertion testing results showed that, similar to the Si-NEs, the ECM-NEs were naturally sufficiently rigid for implantation without external aids, whereas flexible PDMS-NEs could not be directly implanted. At an insertion speed of 100 μm s^{-1}, the shank of the ECM-NEs started to hydrate, resulting in buckling of the uninserted portion of the device at an insertion depth of approximately 1.8 mm (Figure 4). At higher insertion speeds (300 μm s^{-1} and 500 μm s^{-1}), the full shank was successfully inserted and no buckling occurred. In this study, an insertion speed of 500 μm s^{-1} was used for all *in vivo* implantations for the tissue studies and neural recordings.

Strain fields at the tissue–device interface

It is suggested that, after implantation, the motion of the NEs in the brain induces strains in the area around the NEs owing to the mechanical mismatch between the brain and the implanted NEs. This effectively causes post-insertion injury of the tissue and blood vessels, resulting in inflammation and glial scar

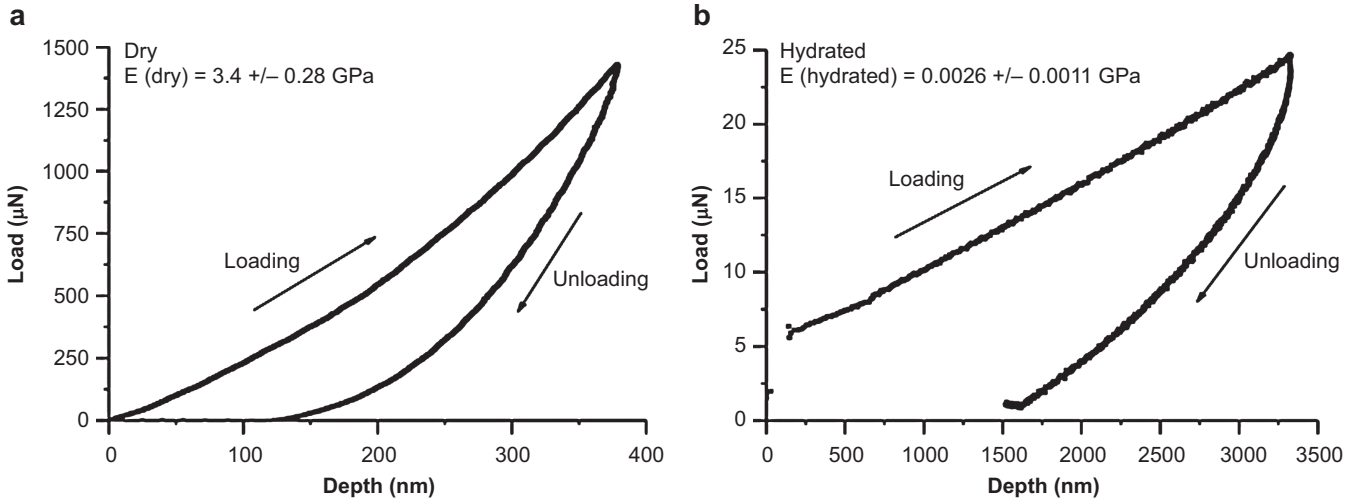

Figure 3 Nano-indentation results for: (**a**) dry collagen films; (**b**) hydrated collagen films.

encapsulation around the NEs and isolating neurons from the NEs, thus reducing the electrodes' ability to reliably record neural signals[21,31,45]. Once implanted, the ECM-NEs soften by hydration (E of hydrated collagen film ≈ 2.64 ± 1.1 MPa (Figure 3b), and E of hydrated Matrigel ≈ 450 Pa[46]), reducing the mechanical mismatch between the brain and the NEs, which could result in a lower interfacial strain field and potentially lead to reduced encapsulation of the NEs. To elucidate the strains in the tissue caused by motions of different types of NEs and to investigate which NE induces less strain and, thus, potentially causes less damage to the brain, we carried out finite element method (FEM) simulations on brain tissue implanted with three categories of NEs of the same dimensions: ECM-NEs, a synthetic ultra-flexible analog (PDMS-NE with the same dimensions made from ultra-flexible synthetic PDMS materials), and a synthetic stiff analog (Si-NE with the same dimensions made from stiff synthetic Si materials). Si-NEs and PDMS-NEs each contact the brain with an estimated low physical contact (friction) coefficient (f) of 0.04[47–49]. A series of ECM-NEs/brain coupling conditions, ranging from f = 0.04 to 1.00, as well as a perfect bond

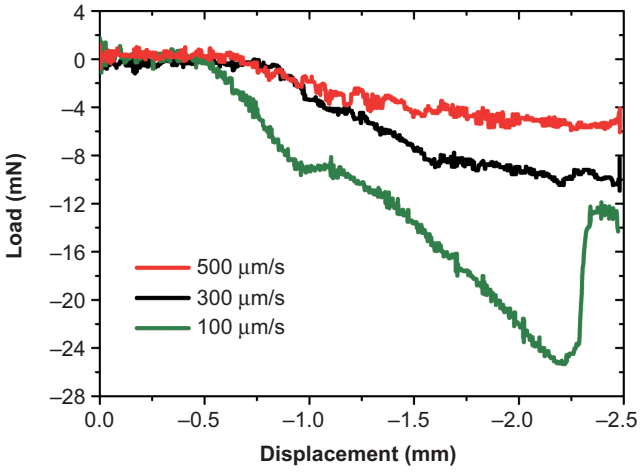

Figure 4 Insertion force as a function of microelectrode position. The insertion speed affects the resulting force and maximum insertion depth.

condition (i.e., positional continuity between the ECM and the embedding tissue at all strains) were studied. The large surface displacement in anesthetized rats, due to respiration, was found to be under 30 μm, whereas the much smaller surface displacement in the anesthetized rat due to vascular pulsations was found to be 1–4 μm[50]. Goldstein and Salcman estimated that a relative motion of 6 μm between NEs and the brain tissue could cause neuronal recording signals to be lost in noise[21]. In this study, a 6 μm displacement was adopted. The motions of an NE in its axial direction (y direction) and lateral directions (x direction and z direction, directions perpendicular to the NE) were studied. Motions in the lateral direction induce large strain fields close to the surface of the brain, whereas nearly zero strain fields are observed at the electrode tip (where all the recording sites are located), as shown in Figure 5a and b. Motion in the axial direction induces strain fields in which the maximum strains occur at the electrode tip (i.e., close to the recording sites), potentially causing more reactive tissue responses in this area (Figure 5c and d, and Supplementary Figures S4–S6). Therefore, detailed results for the latter case are analyzed and presented (Figure 5). Figure 5e and f shows the strain distributions in response to a 6 μm forward displacement (i.e., increasing depth into the brain tissue) for the three types of NEs, from the NE tip in the brain along the x direction and along the brain–NE interfaces at the axial direction (centerline) of the NEs, respectively. With the same physical coupling conditions (f = 0.04), the maximum strains induced by the ECM-NEs and PDMS-NEs are 3.4% and 8.5% lower than that induced by the Si-NEs, respectively. This result agrees with the conclusion reported by Kipke *et al.*[12]. Further, given the observation that neural cells infiltrate ECM materials[23,29,30,51], it is reasonable to expect that the physical coupling between the ECM and brain tissue is significant. No previous study of the friction/bonding between ECM material and brain tissue was found, but the f between bone and muscle tissue, and the f at the surface of tissue engineered cartilage has a much higher value than that of the metal and PDMS materials[49,52–54]. The FE results show that a higher f corresponds to lower strains at the electrode tip (Figure 5e and f). The maximum strain in the perfect bond case is 23% smaller than that in the minimum coupling case (f = 0.04), whereas it is 20% smaller than that induced by the PDMS-NEs, and it is 26% smaller than that induced by the Si-NEs. Figure 5c and d shows the strain fields for a low physical coupling case (f = 0.04) and a perfect bonding case. Compared with the low physical

doi:10.1038/micronano.2015.10

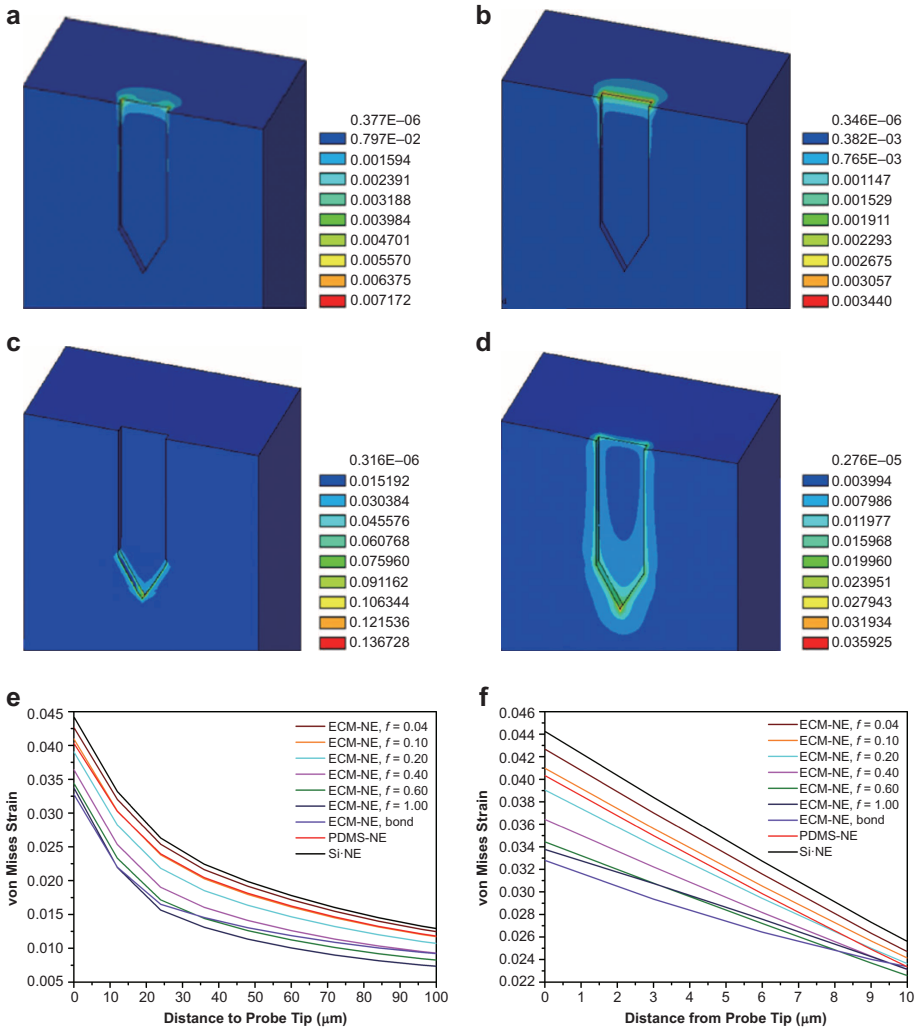

Figure 5 (**a**) and (**b**) FEM results showing the von Mises strain distribution in the brain resulting from a 6 μm displacement of the ECM-NEs in the *x* direction with: (**a**) a low NE-brain coupling coefficient of 0.04; (**b**) a perfect bond condition. (**c**) and (**d**) FEM results of the strains induced in the brain tissue in response to a 6 μm forward displacement in the axial direction with: (**c**) a low coupling coefficient of 0.04 and (**d**) a perfect bond condition. (**e**) Summary of the resultant strains from the NE tip along the brain–NE interfaces in the axial direction (centerline) of the NEs. (**f**) Summary of the resultant strains from the NE tip in the brain along the *x* direction.

coupling case, the perfect bonding case shows an increased strain along the sidewall while relieving strain near the electrode tip. This is because most of the deformation and thus the strain have occurred in the sidewall for the cases with higher *f* or perfect bonding. Compared with conventional stiff NEs and soft NEs made from synthetic materials (such as PDMS), the ECM-NEs benefit from having a low mechanical modulus and thereby reducing the mechanical mismatch between the tissue and the NEs, as well as from being neuron-integrative by enhancing the attachment between the NEs and the brain tissue, which results in reduced strain in the surrounding tissue and thereby potentially reduces injury to the brain and encapsulation of the NEs.

Electrophysiological recording

In vivo neuronal recording experiments using a rat model demonstrated the functionality of these ECM-NEs (Figure 6). The tests involved an anesthetized rat with its head fixed in a stereotaxic apparatus, and the ECM-NEs were implanted into Layer IV of the barrel cortex. Acute neural recordings were acquired immediately after the electrode implantation. The devices successfully acquired multi-channel signals and recorded multi-unit neuron spikes from the barrel cortex following a mechanical stimulation of the whiskers. Figure 6a shows a representative recording trace of neural signals acquired continually over a 90 s time period, and Supplementary Figure S7 shows the corresponding power spectral density. Figure 6c and d shows the sorted principal components, the multi-unit activity, the mean waveforms and the ISI histograms of each cluster. The SNR of this recording is 3.32. Overall, these data demonstrated the ability to directly implant the ECM-NEs into the target brain region and record multi-unit neural activity from viable neurons located close to the NEs.

Initial extended-time neural recording studies suggest that these ECM-based NEs maintained their recording capability over a five-week time period. The *in vivo* EIS were stable over four weeks after implantation. Figure 6e–h shows a representative two-week recording from whisker stimulation. The mean SNR of the ECM-based electrodes (Figure 6i) were comparable to those from the commercial electrodes.

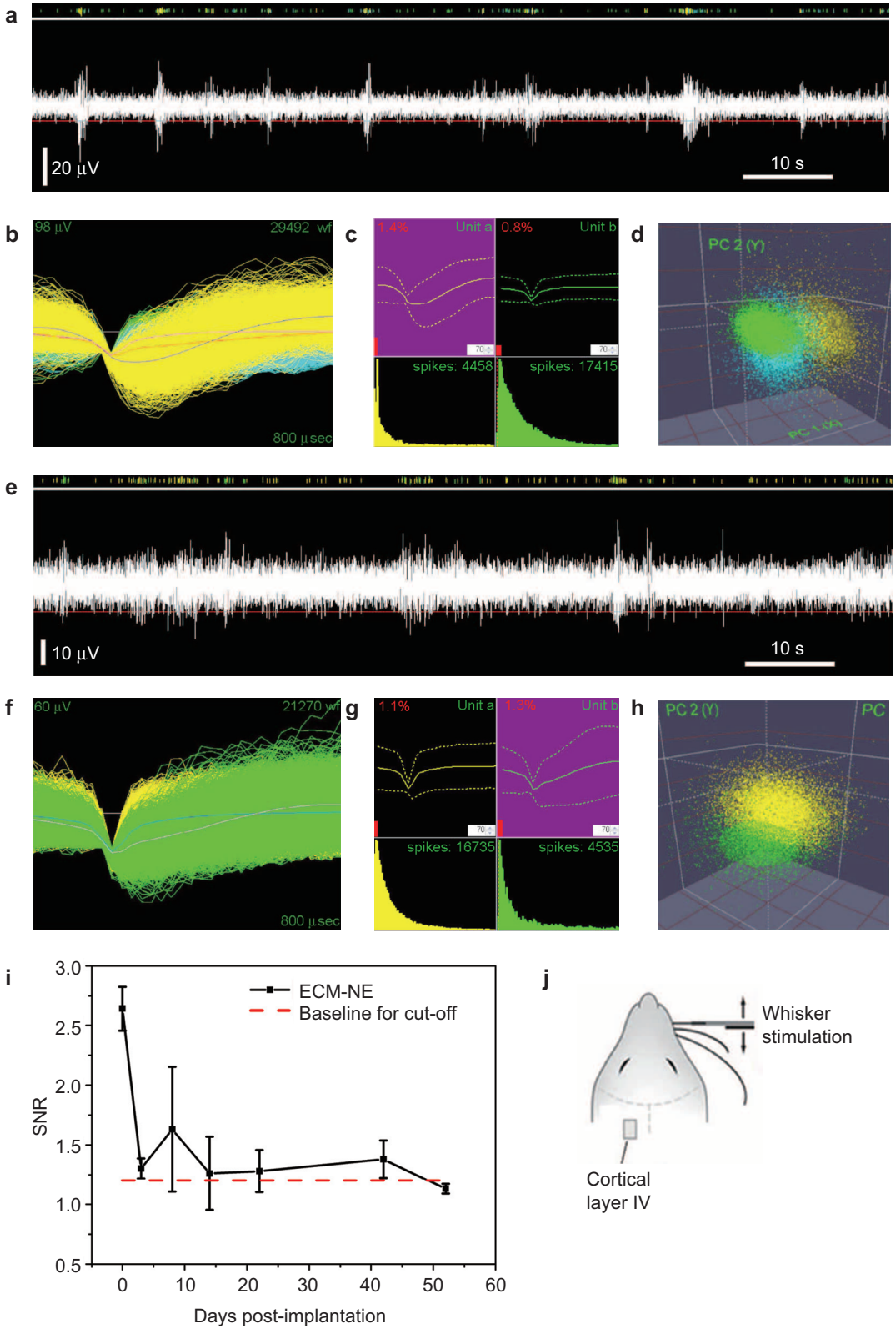

Figure 6 Neural signal recording data from animal validation experiments showing *in vivo* electrophysiological recording capabilities of the ECM microelectrodes. (**a**) and (**d**) day 0 results: (**a**) representative 90 s of high-speed recording showing neural spikes upon whisker stimulation, (**b**) overlay of neural recordings within a 0.8 ms time window, (**c**) mean waveform and ISI histology, and (**d**) results from PCA showing the three clusters. (**e**)–(**h**) two-week neural recording: (**e**) representative 90 s of high-speed recording showing neural spikes upon whisker stimulation, (**f**) overlay of neural recordings within a 0.8 ms time window, (**g**) mean waveform and ISI histology, and (**h**) results from PCA showing the three clusters, (**i**) mean SNR of the largest signal over a 54-day time period, and (**j**) overview of the stimulation experiment, showing the location of the ECM-NEs and a schematic of the whisker stimulation.

doi:10.1038/micronano.2015.10

Tissue histology analysis

Histological studies demonstrated that the chronically implanted ECM-NEs show a qualitatively reduced tissue response compared with the synthetic ultra-flexible analog (PDMS-NEs) (Figure 7). Sixteen weeks after implantation, the ECM-NEs elicited a lesser reactive astrocyte response including glial fibrillary acidic protein and chondroitin sulfate proteoglycans (as shown in CS56 staining) formation (compared with PDMS-NEs, student's *t*-test, $p < 0.05$), implying lesser glial scarring at the brain tissue–NE interfaces. In addition to the effect of glial scarring that could impede the electrical signaling at the brain–NE interfaces, the ability of the NEs to record signals from neurons is directly related to the proximity of viable neurons at the interfaces. As shown in Figure 8, a significantly large number of viable neurons (as shown in $NeuN^+$ staining) and a higher neuronal density were observed in the ROI surrounding the insertion site of the chronically implanted ECM-NEs (compared with PDMS-NEs, student's *t*-test, both $p < 0.05$). These tissue response results indicate that in comparison with the NEs constituted of the synthetic materials (e.g., PDMS), the ECM-NEs could be better tolerated by the brain.

DISCUSSION

Electrically functional NEs composed primarily of ECM proteins are achieved by protein hydrogel microfabrication and implementation technologies. In contrast to previous approaches, which featured nano-scale ECM coatings on electrodes largely comprising foreign materials, these ECM-NEs feature the introduction of minimal foreign materials into the brain tissue. As demonstrated in the tissue histological studies, the ECM-NEs elicit reduced inflammatory responses and increased neuron cell densities around the implanted devices compared with a synthetic analog. Further, based on the fact that natural ECM proteins serve as a matrix and reservoir for varieties of cell adhesion molecules, signaling molecules, and therapeutic molecules (e.g., integrins, proteoglycans), these ECM structures could be modified with neural molecules in the future to provide devices with additional functions such as further improving cell/tissue adhesion, controlling cell growth, migration, signaling, targeting, and therapeutics.

In addition to their neural biocompatibility and owing to the mechanically adaptive characteristics of the ECM proteins (especially collagens), these proteins serve as a major structural material to fulfill the needs for both successful implantation during surgery and improved tissue-compliance post-surgery to reduce mechanical stresses on the neural tissue, thereby minimizing mechanical compatibility issues. Although the present data are encouraging in improving neuron cell attachments and thus reducing inflammation and strain fields at the device–tissue interfaces in comparison to a synthetic stiff analog and a

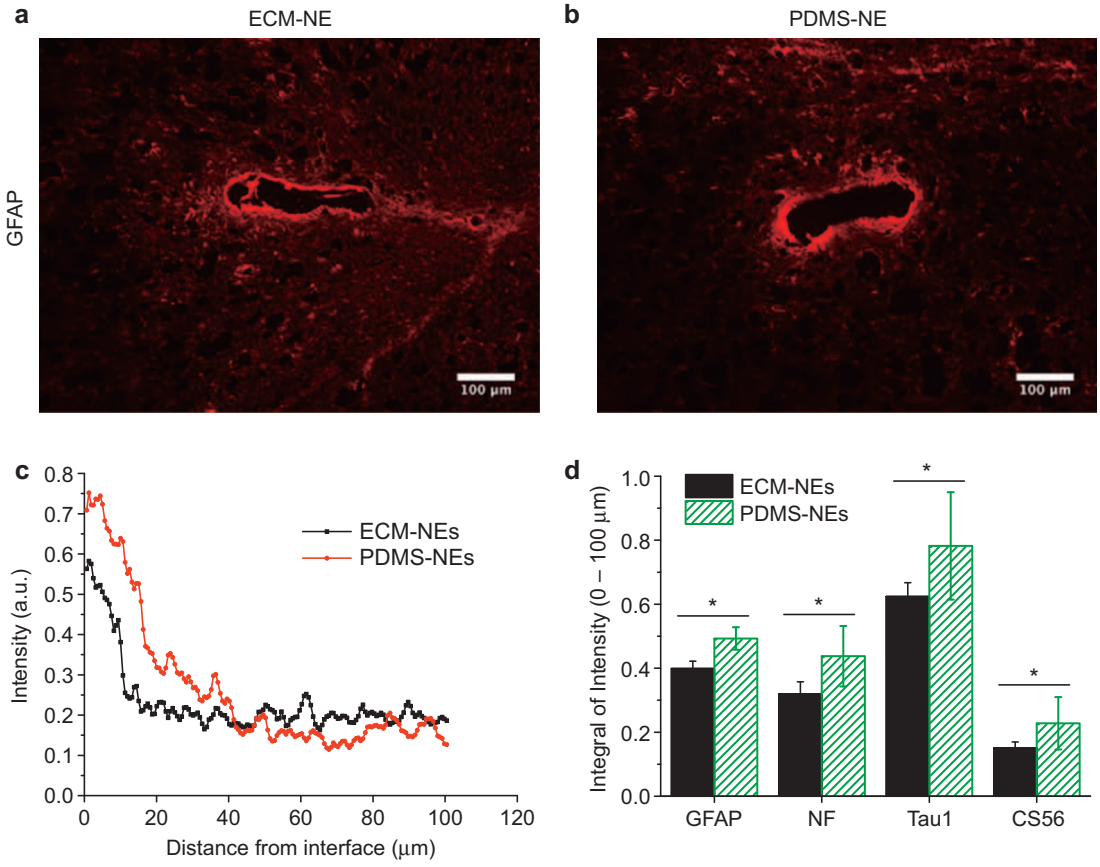

Figure 7 Histology of tissue response to chronically implanted NEs. (**a**) and (**b**) immunohistochemically marked glial fibrillary acidic protein (GFAP) in the tissue that had been implanted with NEs for 16 weeks: (**a**) ECM-NEs, (**b**) PDMS-NEs; (**c**) average image intensities of immunohistochemically marked GFAP were computed up to a distance of 100 µm from the brain tissue–device interface. (**d**) Integrated image intensities of immunohistochemical markers for the reactive astrocyte responses were computed up to a distance of 100 µm from the brain tissue–NE interface. Significant differences observed between the ECM-NEs and PDMS-NEs in the integrated image intensities of immunohistochemical markers are represented by *, indicating $p < 0.05$.

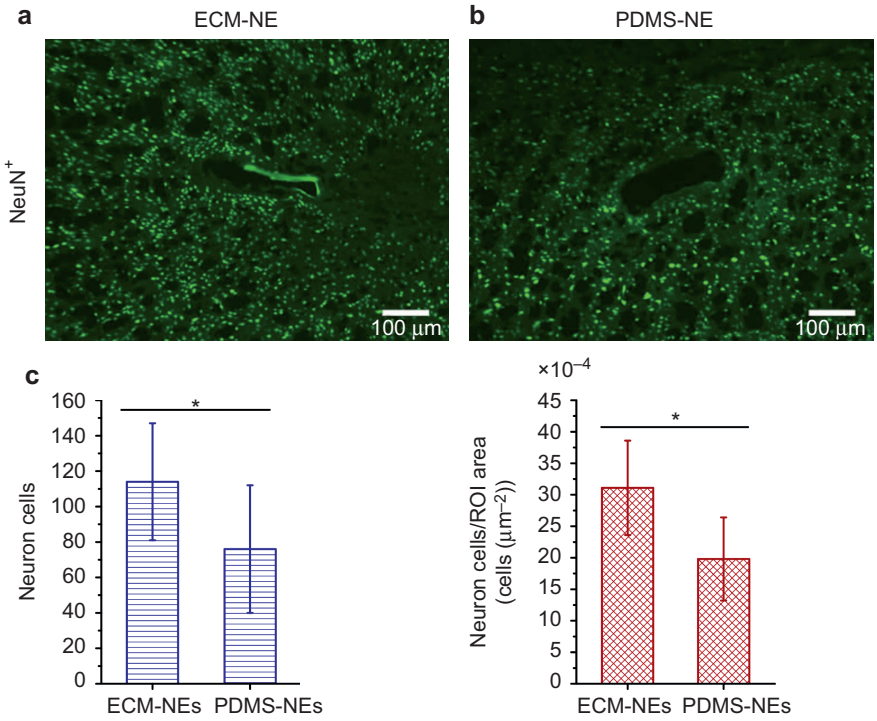

Figure 8 Representative images of NeuN$^+$ stained neuronal nuclei in tissue that had been implanted with NEs for 16 weeks: (**a**) ECM-NEs and (**b**) PDMS-MEs; (**c**) comparison of total viable neuron counts and neuron densities within the ROI (100 μm from each insertion site). Significant differences observed between the ECM-NEs and PDMS-NEs in the total viable neurons and neuron densities are presented by *, indicating $p < 0.05$.

synthetic flexible analog, the overall width of the current device is 310 μm, which is greater than the feature sizes of neurons and the size of the blood–brain barrier (BBB). Moreover, hydration of the devices after implantation causes swelling of the ECM materials, thus enlarging the device footprint in the neural tissue and creating a significant potential for damage to neuron cells and the BBB, thereby increasing initial damage and inflammation. Present efforts are focused on reducing the width of the ECM-NEs to achieve dimensions comparable to the feature sizes of neurons and BBB structures (e.g., the diameter of a neuron cell is approximately 20 μm) that also provide sufficient ECM materials to support chronic neural interfaces. Multiple shanks are also desired to interface with neurons at multiple locations. The fabrication process developed for the ECM-NEs is compatible with the multiple shank scenario, with the minimum distance between two adjacent shanks being determined by the excimer laser fabrication on the order of tens of microns.

Although purely passive intracortical NE systems for recording multi-unit activities from rat barrel cortices have been used to demonstrate the capabilities of the ECM-NEs, the same approaches are compatible with fully active systems. Moreover, by reducing the sizes of the recording sites while controlling their impedance values (less than 1~2 MΩ at 1 kHz[55]), recordings from single unit activities could be achieved.

CONCLUSIONS

This study reports a new materials strategy for NPDs that relies on the use of ECM proteins as the major structural materials. Microfabrication processes and an implementation approach have been developed to pattern ECM proteins with microelectronic devices. As a case study, a collagen- and Matrigel-based intracortical NE is demonstrated. This ECM-based microfabrication and integration approach may yield fundamental advances in the development of NPDs, leveraging material biocompatibility, mechanical robustness for tissue interfacing, and neural signaling capability. A comparison study demonstrated that the ECM-NEs exhibited improved biocompatibility with neural tissue over synthetic analogs. After being implanted for 16 weeks, the ECM-NEs showed less reactive astrocyte responses including glial fibrillary acidic proteins and chondroitin sulfate proteoglycans compared with PDMS-NEs. These favorable results were attributed to the reduction of foreign materials introduced into the brain and to the mechanically adaptive characteristic of the ECM-NEs. Unlike an ultra-flexible analog that buckled and thus could not be inserted, at 500 μm s^{-1} insertion speed, the ECM-NE could be inserted to a depth of up to 1.8 mm with a maximum load of less than 6 mN. After implantation, the ECM-NEs softened by hydration, forming a more tissue-compliant interface. An FEM analysis demonstrated that the maximum strain induced by an ECM-NE could be up to 26% lower than that induced by a synthetic stiff analog. In addition, we validated the *in vivo* functionality of the ECM-NEs by electrophysiological recordings from the rat barrel cortex, showing that the ECM-NEs are capable of monitoring multi-unit activity upon whisker stimulation. Beyond intracortical neural recording systems, the ECM-based microfabrication and integration approaches provide numerous potential applications in NPDs and neural interfaces. The merging of microfabrication technologies and natural products such as ECM materials is expected to yield benefits in additional applications where biocompatibility, small feature sizes, and electrical and mechanical functionality are of interest.

doi:10.1038/micronano.2015.10

ACKNOWLEDGEMENTS

We thank S. Rajaraman for help in using the facilities at Axion Biosystems, Inc., Atlanta, GA, USA for Pt-black coating. This work was funded by the Defense Advanced Research Projects Agency (DARPA) MTO under the auspices of Dr. Jack Judy through the Space and Naval Warfare Systems Center, Pacific Grant/Contract No. N66001-11-1-4014.

COMPETING INTERESTS

The authors declare no competing financial interest.

REFERENCES

1 Velliste M, Perel S, Spalding MC *et al.* Cortical control of a prosthetic arm for self-feeding. *Nature* 2008; **453**: 1098–1101.
2 Williams JC, Rennaker RL, Kipke DR. Long-term neural recording characteristics of wire microelectrode arrays implanted in cerebral cortex. *Brain Research Protocols* 1999**; 4**: 303–313.
3 Nordhausen CT, Maynard EM, Normann RA. Single unit recording capabilities of a 100 microelectrode array. *Brain Research* 1996; **726**: 129–140.
4 Donoghue JP. Connecting cortex to machines: recent advances in brain interfaces. *Nature Neuroscience* 2002; **5**: 1085–1088.
5 Nicolelis MA. Brain–machine interfaces to restore motor function and probe neural circuits. *Nature Reviews Neuroscience* 2003; **4**: 417–422.
6 Schwartz AB. Cortical neural prosthetics. *Annual Review of Neuroscience* 2004; **27**: 487–507.
7 Hochberg LR, Serruya MD, Friehs GM *et al.* Neuronal ensemble control of prosthetic devices by a human with tetraplegia. *Nature* 2006; **442**: 164–171.
8 Lee K, He J, Singh A *et al.* Polyimide based neural implants with stiffness improvement. *Sensors and Actuators B: Chemical* 2004; **102**: 67–72.
9 Kuo J, Kim BJ, Hara SA *et al.* Fabrication of 3D parylene sheath probes for reliable neuroprosthetic recordings. Solid-State Sensors, Actuators, and Microsystems Workshop; 3-7 Jun 2012; Hilton Head Island, SC, USA; 2012: 30–33.
10 Summary of Properties for Kapton® Polyimide Films. DuPont, Wilmington DE, 1987.
11 Parylene Specifications. VSI Parylene, Louisville, CO, USA.
12 Subbaroyan J, Martin DC, Kipke DR. A finite-element model of the mechanical effects of implantable microelectrodes in the cerebral cortex. *Journal of Neural Engineering* 2005; **2**: 103–113.
13 Sridharan A, Nguyen JK, Capadona JR *et al.* Compliant intracortical implants reduce strains and strain rates in brain tissue *in vivo*. *Journal of Neural Engineering* 2015; **12**: 036002.
14 O'Brien DP, Nichols TR, Allen MG. Flexible microelectrode arrays with integrated insertion devices. The 14th IEEE International Conference on Micro Electro Mechanical Systems(MEMS 2001); 21-25 Jan 2001; Interlaken, Switzerland; 2001; 216–219.
15 Rousche PJ, Normann RA. A method for pneumatically inserting an array of penetrating electrodes into cortical tissue. *Annals of Biomedical Engineering* 1992; **20**: 413–422.
16 Chen P. Ultrasonic Neural Probe for Real Time Electromechanical Histology of Neural Interfaces. 2012 Solid State Sensors and Actuators Workshop; 3-7 Jun, 2012; Hilton Head Island, SC, USA; 2012.
17 Jorfi M, Skousen JL, Weder C *et al.* Progress towards biocompatible intracortical microelectrodes for neural interfacing applications. *Journal of Neural Engineering* 2015; **12**: 011001.
18 Weder C, Capadona JR, Shanmuganathan K *et al.* Bio-inspired mechanically-adaptive nanocomposites. *Polymer Preprints (American Chemical Society, Division of Polymer Chemistry)* 2010; **51**: 269–270.
19 Potter-Baker KA, Capadona JR. Reducing the "Stress": antioxidative therapeutic and material approaches may prevent intracortical microelectrode failure. *ACS Macro Letters* 2015; **4**: 275–279.
20 Bellamkonda RV, Pai SB, Renaud P. Materials for neural interfaces. *MRS Bulletin* 2012; **37**: 557–561.
21 Goldstein SR, Salcman M. Mechanical factors in the design of chronic recording intracortical microelectrodes. *IEEE Transactions on Biomedical Engineering* 1973; **20**: 260–269.
22 Polikov VS, Tresco PA, Reichert WM. Response of brain tissue to chronically implanted neural electrodes. *Journal of Neuroscience Methods* 2005; **148**: 1–18.
23 Chen S, Allen MG. Extracellular matrix-based materials for neural interfacing. *MRS Bulletin* 2012; **37**: 606–613.
24 Sanes JR. Extracellular matrix molecules that influence neural development. *Annual Review of Neuroscience* 1989; **12**: 491–516.
25 Rauch U. Extracellular matrix components associated with remodeling processes in brain. *Cellular and Molecular Life Sciences CMLS* 2004; **61**: 2031–2045.
26 Tonge D, Golding JP, Edbladh M *et al.* Effects of extracellular matrix components on axonal outgrowth from peripheral nerves of adult animals *in vitro*. *Experimental Neurology* 1997; **146**: 81–90.
27 Labrador RO, Butí M, Navarro X. Influence of collagen and laminin gels concentration on nerve regeneration after resection and tube repair. *Experimental Neurology* 1998; **149**: 243–252.
28 He W, McConnell GC, Bellamkonda RV. Nanoscale laminin coating modulates cortical scarring response around implanted silicon microelectrode arrays. *Journal of Neural Engineering* 2006; **3**: 316.
29 Chen YS, Hsieh CL, Tsai CC *et al.* Peripheral nerve regeneration using silicone rubber chambers filled with collagen, laminin and fibronectin. *Biomaterials* 2000; **21**: 1541–1547.
30 Tibbitt MW, Anseth KS. Hydrogels as extracellular matrix mimics for 3D cell culture. *Biotechnology and Bioengineering* 2009; **103**: 655–663.
31 Mukhatyar V, Karumbaiah, L, Yeh J *et al.* Tissue engineering strategies designed to realize the endogenous regenerative potential of peripheral nerves. *Advanced Materials* 2009; **21**: 4670–4679.
32 Abidian MR, Martin DC. Multifunctional nanobiomaterials for neural interfaces. *Advanced Functional Materials* 2009; **19**: 573–585.
33 Kozai TDY, Langhals NB, Patel PR *et al.* Ultrasmall implantable composite microelectrodes with bioactive surfaces for chronic neural interfaces. *Nature Materials* 2012; **11**: 1065–1073.
34 He W, McConnell GC, Schneider TM *et al.* A novel anti-inflammatory surface for neural electrodes. *Advanced Materials* 2007; **19**: 3529–3533.
35 Cui X, Wiler J, Dzaman M *et al. In vivo* studies of polypyrrole/peptide coated neural probes. *Biomaterials* 2003; **24**: 777–787.
36 De Faveri S, Maggiolini E, Miele E *et al.* Bio-inspired hybrid microelectrodes: a hybrid solution to improve long-term performance of chronic intracortical implants. *Frontiers in Neuroengineering* 2014; **7**: 7.
37 Naik N, Kumar V, Chaikof EL *et al.* MEMS-assisted spatially homogeneous endothelialization of a high length-to-depth aspect ratio microvascular network. Proceedings of Annual International Conference on IEEE Engineering in Medicine and Biology Society (EMBC 2011; 29 Aug-3 Sep 2011; Boston, MA, USA; 2011: 290–293.
38 Caves JM, Kumar VA, Xu W *et al.* Microcrimped collagen fiber-elastin composites. *Advanced Materials* 2010; **22**: 2041–2044.
39 Gillette BM, Jensen JA, Tang B *et al.* In situ collagen assembly for integrating microfabricated three-dimensional cell-seeded matrices. *Nature Materials* 2008; **7**: 636–640.
40 Phillips JB, Bunting SC, Hall SM *et al.* Neural tissue engineering: a self-organizing collagen guidance conduit. *Tissue Engineering* 2005; **11**: 1611–1617.
41 Karumbaiah L, Saxena T, Carlson D *et al.* Relationship between intracortical electrode design and chronic recording function. *Biomaterials* 2013; **34**: 8061–8074.
42 Saxena T, Karumbaiah L, Gaupp EA *et al.* The impact of chronic blood–brain barrier breach on intracortical electrode function. *Biomaterials* 2013; **34**: 4703–4713.
43 Gautieri A, Vesentini S, Redaelli A *et al.* Hierarchical structure and nanomechanics of collagen microfibrils from the atomistic scale up. *Nano Letters* 2011; **11**: 757–766.
44 Rebscher SJ, Hetherington A, Bonham B *et al.* Considerations for the design of future cochlear implant electrode arrays: electrode array stiffness, size and depth of insertion. *Journal of Rehabilitation Research and Development* 2008; **45**: 731–747.
45 McConnell GC, Rees HD, Levey AI *et al.* Implanted neural electrodes cause chronic, local inflammation that is correlated with local neurodegeneration. *Journal of Neural Engineering* 2009; **6**: 056003.
46 Soofi SS, Last JA, Liliensiek SJ *et al.* The elastic modulus of Matrigel™ as determined by atomic force microscopy. *Journal of Structural Biology* 2009; **167**: 216–219.
47 Ching HA, Choudhury D, Nine MJ *et al.* Effects of surface coating on reducing friction and wear of orthopaedic implants. *Science and Technology of Advanced Materials* 2014; **15**: 014402.
48 Rashid B, Destrade M, Gilchrist MD. Determination of friction coefficient in unconfined compression of brain tissue. *Journal of the Mechanical Behavior of Biomedical Materials* 2012; **14**: 163–171.
49 Chawla K, Lee S, Lee BP *et al.* A novel low-friction surface for biomedical applications: Modification of poly (dimethylsiloxane) (PDMS) with polyethylene glycol (PEG)-DOPA-lysine. *Journal of Biomedical Materials Research Part A* 2009; **90**: 742–749.
50 Muthuswamy J, Saha R, Gilletti A. Tissue micromotion induced stress around brain implants. 3rd IEEE/EMBS Special Topic Conference on Microtechnology in Medicine and Biology; 12-15 May 2005; Oahu, HI, USA; 2005; 102–103.
51 Parenteau-Bareil R, Gauvin R, Berthod F. Collagen-based biomaterials for tissue engineering applications. *Materials* 2010; **3**: 1863–1887.
52 Grad S, Loparic M, Peter R *et al.* Sliding motion modulates stiffness and friction coefficient at the surface of tissue engineered cartilage. *Osteoarthritis and Cartilage* 2012; **20**: 288–295.
53 Plainfosse M, Hatton P, Crawford A *et al.* Influence of the extracellular matrix on the frictional properties of tissue-engineered cartilage. *Biochemical Society Transactions* 2007; **35**: 677–679.

54 Ritter RC, Quate EG, Gillies GT *et al*. Measurement of friction on straight catheters in *in vitro* brain and phantom material. *IEEE Transactions on Biomedical Engineering* 1998; **45**: 476–485.
55 Zhang H, Patel PR, Xie Z *et al*. Tissue-compliant neural implants from microfabricated carbon nanotube multilayer composite. *ACS Nano* 2013; **7**: 7619–7629.

Supplementary information for this article can be found on the *Microsystems & Nanoengineering* website (http://www.nature.com/micronano).